Toward Industry-Standard Flow-Induced Noise Prediction

G. Guilloud[1], P. Martinez[2], J. Golliard[3], C. Schram[4]

[1] *TNO Science & Industry, Delft, The Netherlands, Email: geraud.guilloud@tno.nl*

[2] *LMS International, Leuven, Belgium, Email: paula.martinez@lmsintl.com*

[3] *TNO Science & Industry, Delft, The Netherlands, Email: joachim.golliard@tno.nl*

[4] *LMS International, Leuven, Belgium, Email: christophe.schram@lmsintl.com*

Introduction

Despite the aeroacoustic expertise reached nowadays in air and ground transportation, energy sector or domestic appliances, the decibel accuracy of an acoustic prediction for industrial cases is still challenging. Strong investments are made nowadays by oil and gas companies to determine and reduce the sound produced by flow inside industrial ducts, such as pipelines or gasoduct. HVAC noise reduction in a car has become a strong condition of comfort for passengers and then a concern for car manufacturer. This paper tackles the flow-induced noise prediction of an industrial case and the computational optimization based on the acoustic analogy. The authors will focus on key points of the numerical procedure representing possible sources of errors for noise prediction.

In the first section the geometry, the flow and the acoustic description are presented. In the second section, some possible optimizations of the procedure are presented.

Flow and flow induced-noise across a slit diaphragm

The geometry of interest is presented in Figure 1. It consists of a duct with a square cross-section $D \times D$ with $D = 0.3$ m and a centered slit diaphragm of area $(D/3 \times D)$ m^2. The diaphragm thickness is $D/100$. The geometry is based on an experimental study carried out by Nelson and Morfey [1]. They performed series of experiments to measure and normalize the power radiated by the flow through a diaphragm. They used different geometries of rectangular diaphragms within a duct with a square cross-section and they normalized the Sound Power radiated both below and above the cut-off frequency of the duct.

This paper will focus on the configuration with a fully developed turbulent flow with a Reynolds based on the duct side length of $Re = 4.65 \times 10^5$ and a Mach number of $M = 0.04$. This corresponds to a turbulent velocity profile with an average velocity of 15.6 m/s. The reference velocity used in this paper corresponds to the ratio of volume flow rate by the diaphragm aperture surface A_C:

$$U_C = \frac{q}{A_C} = 47.2 m/s. \quad (1)$$

In the following, the inlet is considered anechoic while the outlet consists of an open termination. The purpose

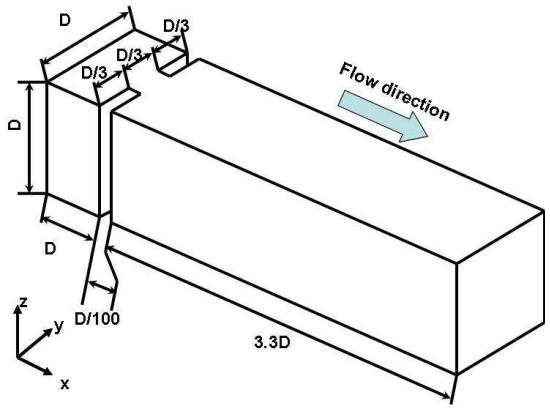

Figure 1: Diaphragm geometry. $D = 0.3$ m.

of this study is the prediction of the Sound Power Level (SWL) transmitted outside the duct.

Doak [2] relates the sound power radiated by sources in an infinite hardwalled duct to the fluctuating forces distribution. Nelson and Morfey's experiments confirmed it in their study [1]. They demonstrated and measured the direct link between the fluctuating drag exerted by the diaphragm and the radiated sound power for a finite hard-walled duct at low Mach number. In Nelson and Morfey's study [1], the geometry, the flows parameters and the drag coefficient were used to normalize the radiated Sound Power Level which was measured in a reverberant chamber situated at the outlet 15 to 20 diameters downstream of the diaphragm. In the same fashion, in this paper, the fluctuating non-dimensional drag on the diaphragm walls is assumed to be the main source of sound for the geometry shown in Figure 1. The cut-off frequency of this geometry is 564 Hz.

Numerical procedure

The numerical determination of the acoustic response is based on a two-steps hybrid approach inspired from Curle's analogy [3]. The flow was numerically determined in a first step. The CFD variables, i.e. velocities and pressure fields, served to synthesize the acoustic sources. In the second step, those sources were propagated toward the listener. Due to the low Mach number, the quadrupoles were considered negligible in comparison to the dipoles which were the only type of sources determined in this study.

Flow field calculation

To numerically simulate the flow, an unstructured mesh was constructed, consisting of 1.7 million hexahedral cells. The inlet and outlet ducts lengths were respectively D and $5.5D$ and a $2D$-long sponge zone was introduced at the outlet of the duct (not presented in Figure 1).

A Reynolds Averaged Navier-Stokes (RANS) $k-\epsilon$ simulation was run in a first stage, in order to provide an initial mean turbulent field for an incompressible Large Eddy Simulation (LES), run in a second stage using a Smagorinsky-Lilly subgrid model with the constant value $Cs = 0.1$. The spatial discretization used a second-order centred finite-difference scheme and the imposed CFL was 0.7 [7].

The initial transient of the CFD was evacuated and not taken into account for the acoustic analysis.

More information about the configuration of the CFD computations and the flow fields results can be found in Ref. [4].

Acoustic analysis

The temporal pressure distribution on the walls of the duct and the diaphragm was exported and used as input for the acoustic solver [8]. The pressure information is first mapped on an acoustic mesh. The mapped source data are converted in the Fourier domain with a FFT. The final action was to compute the radiated acoustic power using the Boundary Element Method (BEM). The BEM is solving the Helmholtz equation by using the information on the surfaces.

As previously explained, the quadrupoles in the Curle's analogy are negligible. The dipoles remain the main source of sound and are expressed on the surface from the CFD data. A more complete description of the numerical method can be found in Ref. [5].

Figure 2 shows a fairly good agreement between the simulation and experimental results of Nelson and Morfey [1]. The Strouhal number is based on the total spoiler width $2D/3$ and on the reference velocity U_C (Equation 1). The normalization of the SWL is presented in Ref. [1].

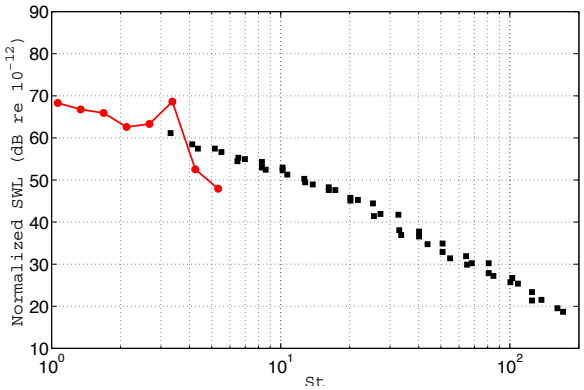

Figure 2: Comparison of the numerical simulations and the experiemental study by Nelson and Morfey [1]. Nelson and Morfey's experiments (■), Numerical simulation (line).

Optimisation

An aspect of concern in industrial applications is the time cost of computations. In an industrial context, running a parametric study to validate the CFD computations or achieving a long sampling time window to describe the source field can be prohibitive. This section will focus on several aspects of the numerical procedure where improvements or assumptions can be made to simplify or fasten the computation without decreasing significantly the global accuracy of the acoustic results.

Use of coarser meshes with a conservative source mapping

In this section, the improvement of the acoustic computation through a conservative source mapping is investigated.

In the hybrid approach, an aspect of concern is the disparity in mesh requirement for the CFD and acoustic calculations. Indeed, as the noise generation is related to the pressure fluctuations, one needs the small variations of pressure which are generated by the small structures of turbulence to obtain an accurate acoustic prediction. This leads to the use of fine meshes in the CFD computations. Such a fine mesh is however not necessary nor desirable for the acoustic computation.

Indeed due to the ratio between the small scales of turbulence and the wavelengths of the resulting sound at low Mach number, the acoustic mesh can be significantly coarser. A common rule of thumb states that 6 to 10 elements per wavelength are required to preserve the numerical accuracy. Then, the information of the pressure between two non-matching meshes has to be mapped in a way which preserves the accuracy of the source description over te range of scales of concern. A similar issue occurs in the case of flow-structure interactions [6].

To investigate this aspect of the numerical procedure, a general presentation of the mapping is given below. The investigation is presented through a pressure field distribution over a surface S spatially discretized with two different meshes. Those mapping schemes are then applied to the diaphragm case. In order to simplify the problem and reduce the CPU effort, the duct walls are treated as if they were radiating directly in free field, i.e. the sound generated is not propagated inside the duct but is directly radiated by a free standing diaphragm.

Mapping schemes and coarser meshes

On a surface S, let p_j be the pressure data on the node j of the CFD mesh and P_k, the pressure on the node k of the acoustic mesh. P corresponds to the continuous pressure distribution.

$$P(\mathbf{x}) \approx \sum_j p_j \phi_j \quad (CFD\ mesh) \tag{2a}$$

$$P(\mathbf{x}) \approx \sum_k P_k \Phi_k \quad (Acoustic\ mesh) \tag{2b}$$

where ϕ_j and Φ_k are the element's shape function respectively on the CFD and acoustic mesh.

The mapping typically requires computing the pressure P_k on each node k of the coarse mesh.

$$P_k = \sum_j p_j \alpha_{jk} \frac{\int_S \phi_j(\mathbf{x}) d^2\mathbf{x}}{\int_S \Phi_k(\mathbf{x}) d^2\mathbf{x}} \tag{3}$$

This mapping is called conservative in this paper when the integral of the pressure sources is conserved.

$$\int_S p_j \phi_j(\mathbf{x}) d^2\mathbf{x} = \int_S P_k \Phi_k(\mathbf{x}) d^2\mathbf{x} \tag{4}$$

Then the coefficient α_{jk} must fulfill the condition

$$\sum_k \alpha_{jk} = 1, \forall j. \tag{5}$$

Different definitions of α_{jk} yield different mapping schemes.

Four different mapping schemes were studied: one element-based scheme and 3 node-based (nearest-node scheme, inverse-distance scheme and function scheme). The equations related to those schemes are developped in Ref. [4]. In the following, only the results obtained with an element-based scheme are presented.

The two coarse meshes contain respectively 5,000 and 500 elements (Figures 3(b) and 3(c)). The pressure field on the reference mesh provided by the first step of the hybrid methods was used as raw data. This pressure field was mapped on the coarser meshes using both conservative and non-conservative schemes. The computed acoustic powers generated by the mapped pressure fields on the two coarser meshes are compared to the reference mesh acoustic power in Figure 4.

For the first coarse mesh of 5,000 elements, both the conservative and non-conservative mapping provide a good agreement for the lower frequency range. For the highest frequencies considered in this section, the non-conservative scheme presents already maximum errors around 2 dB. This reveals that a fine enough mesh keeps the global accuracy of the acoustic prediction.

In the case of the coarsest mesh of 500 elements, the better performance of the conservative mapping is more evident. While the non-conservative scheme provided large overpredictions of the radiated acoustic power, the conservative scheme provides reasonably accurate results in spite of the drastic coarsening of the mesh. The error for the conservative mapping in this case increases towards the highest frequencies as the frequency becomes too high to consider the cells acoustically compact.

Dipole condensation

In this section, only the contribution of the pressure fluctuation on the diaphragm walls is investigated.

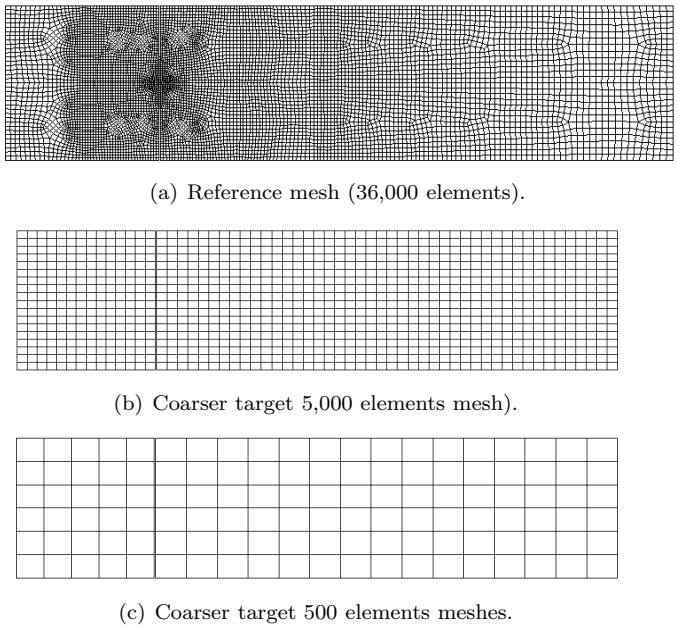

(a) Reference mesh (36,000 elements).

(b) Coarser target 5,000 elements mesh).

(c) Coarser target 500 elements meshes.

Figure 3: Acoustic meshes used for the mapping (top view).

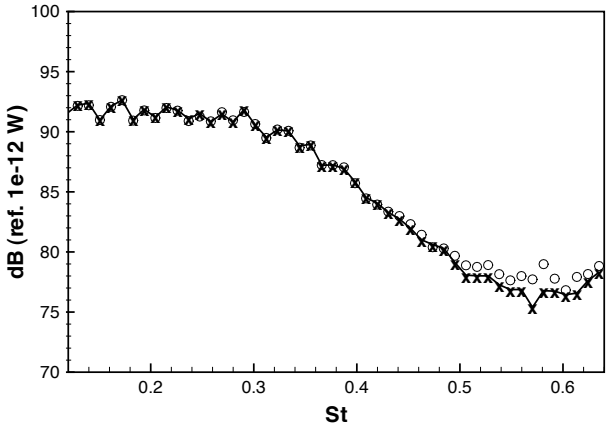

(a) Mesh of 5,000 elements.

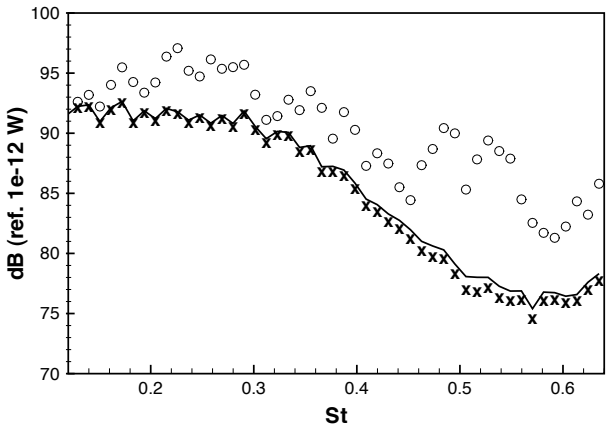

(b) Mesh of 500 elements.

Figure 4: Radiated acoustic power in dB. Reference mesh of 36,000 elements (solid line); non-conservative mapping (○), conservative mapping (×) (Equation 6 of [4]). Strouhal number St based on total spoiler width (0.2 m) and on average velocity at the diaphragm.

In the previous section, the information of pressure was transfered from a CFD node toward an acoustic node. With a compact geometry (i.e a geometry with a low Helmholtz number), the differences of retarded times can be neglected, and the resultant of the source field can be condensed to a single point source. For each frequency, the resulting dipole force is expressed as:

$$\mathbf{F}(\omega) = \sum_{e=1}^{Ne} \frac{1}{4} \sum_{i=1}^{4} P_{ei}(\omega) S_e \vec{\mathbf{n}_\mathbf{e}} \qquad (6)$$

where N_e is the number of quadrilateral elements describing the surface.

This equivalent dipole was inserted in the square duct without the surfaces of the diaphragm. Figure 5 shows the comparison between the sound power levels radiated by a whole field of dipoles and by the corresponding equivalent dipole. Discrepancies with the distributed source results are visible, and their causes are being investigated.

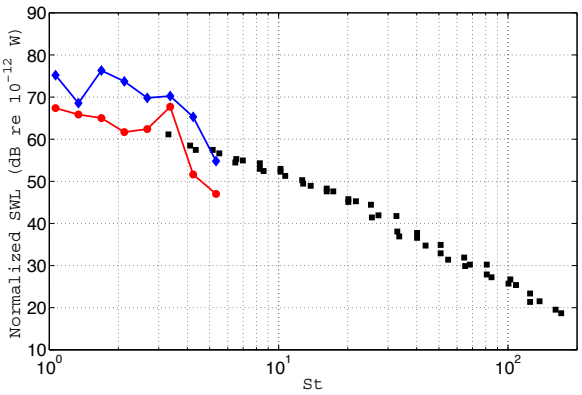

Figure 5: Comparison of the numerical simulations, the experimental study led by Nelson and Morfey [1] and the condensation of dipoles. Nelson and Morfey's experiments (■), Numerical simulation with dipoles field (●), Numerical simulation with equivalent dipole (⧫).

The computation of the Sound Power Radiated for 30 frequencies took 15h for the distribution of dipoles and only 1h30 for the equivalent dipole.

Conclusion

It has been shown that the accuracy of an acoustic prediction based on the aeroacoustical analogy is strongly dependent on the pre-processing of the CFD data.

Firstly, an acoustic procedure based on Curle's analogy has been implemented and tested on Nelson and Morfey's geometry [1]. It has been shown that at low Mach number, the disparity between the CFD and acoustic meshes defines the requirement of an effective conservative mapping.

Secondly, it is possible to condense the dipole field in one equivalent dipole in order to simplify even more the computation, though discrepancies with the distributed sources case are observed in the present work, which are being investigated.

Acknowledgements

The authors gratefully acknowledge the European Commission financial support, provided under the framework of the Marie Curie Research Training Network project AETHER (contract no MRTN-CT-2006-035713).

References

[1] P. A. Nelson, C. L. Morfey. Aerodynamic sound production in low speed flow ducts. Journal of Sound and Vibration **79**(2) (1981), 263-289.

[2] P. E. Doak. Excitation, transmition and radiation of sound from source distributions in hard-walled ducts of finite length. (I): the effects of duct cross-section geometry and source distribution space-time pattern. Journal of Sound and Vibration **31**(1) (1973), 1-72.

[3] N. Curle. The influence of solid boundaries upon aerodynamic sound. Proceeding of the Royal Society of London **A231** (1955), 505–514.

[4] G. Guilloud, P. Martinez-Lera, C. Schram. Optimization of hybrid aeroacoustic computations of an industrial confined flow through mesh coarsening techniques. ISMA Conference (2008), Leuven.

[5] W. Desmet. Boundary Elements Methods in acoustics. ISAAC course (2008), Leuven.

[6] A. de Boer, A. H. van Zuijlen, H. Bijl. Review of coupling methods for non-matching meshes. Computational Methods in Applied Mechanical Engineering **196** (2007), 1515-1525.

[7] ANSYS, Inc. Fluent v6.3 User's Manual (2008).

[8] LMS International. Virtual.Lab User's Guide (2008).